Structural, bonding, dynamical, and electronic properties of liquid silicon: An *ab initio* molecular-dynamics study

I. Štich* and R. Car

International School for Advanced Studies, Strada Costiera 11, Trieste 34014, Italy

M. Parrinello

*IBM Research Division, Forschungslaboratorium Zürich, Rüschlikon 8803, Switzerland
and International School for Advanced Studies, Strada Costiera 11, Trieste 34014, Italy*

We report an extensive first-principles molecular-dynamics study of metallic liquid silicon. Our description of the local order is in excellent agreement with x-ray- and neutron-diffraction experiments. The difference in internal energy between the simulated liquid phase and the crystal agrees well with the experimental enthalpy of melting. Analysis of the valence-electronic-charge density shows persistence of some covalent bonds in the melt. These bonds give rise in the power spectrum of the system dynamics to a well-identifiable feature associated with stretching vibrations. Unlike the case in the crystal, in the liquid the covalent bonds are continuously forming and breaking in response to atomic motion. The majority of bonds are broken on average, leading to fast diffusion and to metallic behavior of the melt. The calculated electronic conductivity shows good agreement with available experimental data.

I. INTRODUCTION

Silicon has several high-density forms which include crystalline (*c*-Si), amorphous (*a*-Si), and liquid (*l*-Si) phases. The former two are, at normal pressure, semiconducting and covalent, while the latter is metallic. The semiconducting Si phases have traditionally received much attention and have become a prototype of elemental semiconductor which has often been used as a testing ground for new theories and methods. The metallic liquid phase, however, was relatively little explored, both experimentally[1-4] and theoretically.[5-9] The crystal-to-liquid transition occurs at a high temperature of ∼1680 K,[10] which makes experiments difficult to make. Yet *l*-Si is technologically important. Single crystals are grown from the liquid phase. Novel dopant profiles are generated by zone refining in laser-melted Si surfaces, and the metallic nature of the melt is used to determine the thickness of the laser-melted region.

l-Si has several intriguing and poorly understood properties. Upon melting, the density of Si increases by ∼10%,[11] and its structure goes from an open structure with coordination number equal to 4 to a more compact liquid structure characterized by a coordination number exceeding 6.[1,2] It is fairly unusual for a liquid metal to have a coordination number between 6 and 7. Most liquid metals are more closely packed with a coordination ∼12.[12] The low coordination of *l*-Si indicates a persistence of covalent bonding in the liquid. A quantitative description of the covalent bonding effects is, however, still missing. The experimentally determined atomic structure of *l*-Si exhibits peculiar features,[1,2] and its static structure factor strongly differs from that characteristic of simple liquid metals, such as, e.g., aluminum.[1]

Upon melting, Si undergoes a semiconductor-to-metal transition as evidenced by a jump in the conductivity by a factor of 20.[10] The ac electrical conductivity has also been measured, and the result indicates a Drude-like behavior,[4] even though the electronic mean free path is short.

The theoretical efforts were concerned mainly with modeling the experimental atomic structure in terms of effective classical potentials[5,6,9,13] or with studying the electronic properties given some model for the atomic structure.[8,9,14] The classical potentials were either constructed empirically by fitting a given set of experimental data[6,13] or derived semiempirically from some approximate theoretical treatment.[5,9] Although often very useful, such approach is not entirely satisfactory since (i) the effective potentials miss the close connection between electronic and atomic structure, (ii) the range of their validity may be limited and is not known in general, and (iii) it is usually difficult to make detailed quantitative predictions for a particular material. For this reason we have studied *l*-Si using an *ab initio* molecular-dynamic (MD) method.[15] In our approach the interatomic forces are obtained from an accurately calculated electronic ground state within density-functional (DF) theory in the local-density approximation (LDA) for exchange and correlation effects.[16] As will be discussed at length in the following, some important qualitative differences emerge between the structures derived from potentials constructed quantum mechanically and those derived from classical empirical potentials.

In this paper the *ab initio* MD approach is applied to an extensive and detailed investigation of structural, dynamical, and electronic properties of *l*-Si. A short version of these results has been presented elsewhere.[17] The structure of our simulated *l*-Si sample is in excellent agreement with the available experimental diffraction

data. Analysis of the electronic charge density allows the first quantitative characterization of covalent bonding effects in the liquid. These appear as local tetrahedral fluctuations that give rise in the power spectrum of the system dynamics to a feature associated with stretching vibrations. The calculated electronic properties are also in good agreement with experiment. The single-particle electronic density of states shows metallic behavior. The calculated ac electrical conductivity compares well with experiment.

The paper is organized as follows: In Sec. II we briefly review the *ab initio* MD scheme and give details of our calculation. In Sec. III we study short-range order and energetics of *l*-Si. Section IV contains a detailed analysis of the bonding properties. Atomic motion is discussed in Sec. V and electronic properties in Sec. VI. Finally, we present our conclusions in Sec. VII. Convergence studies are reported in an Appendix.

II. METHOD AND TECHNICAL DETAILS OF THE SIMULATION

In our MD simulation the ionic forces are derived from the many-body potential $\Phi[\{\mathbf{R}_I\}]$ calculated from the electronic ground state within DF theory. $\Phi[\{\mathbf{R}_I\}]$ defines the Born-Oppenheimer (BO) potential-energy surface for the ions. The electronic ground state is attained by minimizing the energy functional $E[\{\psi_i\}, \{\mathbf{R}_I\}]$ with respect to the "electronic degrees of freedom" $\{\psi_i\}$:

$$\Phi[\{\mathbf{R}_I\}] = \min_{\{\psi_i\}} E[\{\psi_i\}, \{\mathbf{R}_I\}] . \tag{1}$$

The functional $E[\{\psi_i\}, \{\mathbf{R}_I\}]$ is given by[15,18] (using atomic units $e = \hbar = m_e = 1$)

$$
\begin{aligned}
E[\{\psi_i\}, \{\mathbf{R}_I\}] = \sum_i^{\text{occ}} &\int d\mathbf{r}\, \psi_i^*(\mathbf{r})(-\tfrac{1}{2}\nabla^2)\psi_i(\mathbf{r}) \\
&+ \int d\mathbf{r}\, V^{\text{ext}}(\mathbf{r})\rho_e(\mathbf{r}) \\
&+ \frac{1}{2}\int d\mathbf{r}\, d\mathbf{r}' \frac{\rho_e(\mathbf{r})\rho_e(\mathbf{r}')}{|\mathbf{r}-\mathbf{r}'|} \\
&+ E^{\text{xc}}[\rho_e] + \frac{1}{2}\sum_{I \neq J} \frac{Z_I Z_J}{|\mathbf{R}_I - \mathbf{R}_J|} .
\end{aligned} \tag{2}
$$

Here $\rho_e(\mathbf{r})$ denotes the valence electron pseudo-charge-density:

$$\rho_e(\mathbf{r}) = \sum_i^{\text{occ}} |\psi_i(\mathbf{r})|^2 . \tag{3}$$

$V^{\text{ext}}(\mathbf{r})$ is the total ionic pseudopotential acting on the valence electrons, Z_I are ion-core charges, and the state sum extends over the occupied (valence) states. $E^{\text{xc}}[n]$ is the exchange-correlation energy functional,[16] for which we adopt the local-density approximation. The single-particle states $\{\psi_i\}$ are subject to orthonormality constraints:

$$\int d\mathbf{r}\, \psi_i^*(\mathbf{r})\psi_j(\mathbf{r}) = \delta_{ij} . \tag{4}$$

At the minimum of the energy functional, the single-particle states $\{\psi_i\}$ coincide with the so-called Kohn-Sham (KS) orbitals,[19] within a unitary transformation.[15]

The minimization in Eq. (1) can be carried out in different ways, but we find most convenient to follow the generalized Lagrangian formulation of Ref. 15. In order to fix the ionic temperature, we introduce the Nosé thermostat[20] on the ionic degrees of freedom. The system dynamics is governed by the following equations of motion:

$$\mu\ddot{\psi}_i(\mathbf{r},t) = -\frac{\delta E}{\delta \psi_i^*(\mathbf{r},t)} + \sum_j \Lambda_{ij}\psi_j(\mathbf{r},t) , \tag{5a}$$

$$M_I\ddot{\mathbf{R}}_I = -\frac{\partial E}{\partial \mathbf{R}_I} - \frac{M_I}{s}\dot{\mathbf{R}}_I\dot{s} , \tag{5b}$$

$$Q\ddot{s} = s\sum_I M_I(\dot{\mathbf{R}}_I)^2 - sgk_BT + \frac{Q}{s}(\dot{s})^2 . \tag{5c}$$

The Nosé equations (5b) and (5c) are written in terms of "real variables."[20] Therefore, in Eqs. (5) the dot indicates derivative with respect to the "real time."[20] The ions $\{\mathbf{R}_I\}$ move both under the action of interparticle forces [first term on the right-hand side (RHS) of Eq. (5b)] and of the coupling to the thermostat represented by an additional dynamical variable s [second term on the RHS of Eq. (5b)]. The interparticle potential is optimized dynamically via Eq. (5a). Here μ is an arbitrary parameter of appropriate units which serves to define the fictitious classical kinetic energy of the electronic orbitals $\{\psi_i\}$. Λ is a matrix of Lagrange multipliers imposing the orthonormality constraints of Eq. (4). The Nosé thermostat is governed by Eq. (5c), where Q is the dynamical "mass" of the variable s, $g = 3N$, where N is the number of ions, k_B is the Boltzmann's constant, and T is the externally set ionic temperature.

If the potential energy E in Eq. (5b) is given by the BO potential-energy surface Φ, defined in Eq. (1), then, as demonstrated by Nosé,[20] with the above choice of g, Eqs. (5b) and (5c) lead to a canonical distribution in the ionic phase space. One can obtain conditions where this is approximately the case if the electrons, evolving according to Eq. (5a), follow adiabatically the motion of the ions, remaining very close to the ground state. For this to occur the time scale for the motion of the electronic degrees of freedom must be much shorter than that for the ions. The key quantity that controls the electron time scale is μ/E_g, where E_g is the electronic single-particle energy gap. In semiconductors and insulators, E_g is finite and one can select a conveniently small value of μ such that the electronic degrees of freedom acquire only a very small classical kinetic energy to follow adiabatically the ions. In other words, the system stays a long time in a metastable state in which electrons and ions are not in mutual thermal equilibrium, with the electronic temperature being much less than that of the ions. Under these conditions ionic trajectories, initially lying on the BO surface, deviate from it very slowly on the time scale of the MD simulation. Thus very few or no separate minimizations are necessary to keep the system on the BO surface during a MD run. Instead, in systems like metals, where E_g is zero or very close to zero, one cannot effectively decouple ionic and electronic degrees of freedom. In the

present case of liquid Si, which is a metal, we have observed a tendency to thermal equilibration between electronic and ionic subsystems related to the existence of empty electronic states degenerate or nearly degenerate with the occupied states. This induces substantial energy transfer from the ionic to the electronic subsystem. This process cannot be fully eliminated, but may be controlled in part by the choice of μ, since, in a finite-size system, even in a metal, although tiny, E_g is different from zero.

The coupling of electronic and ionic degrees of freedom has two major consequences: (i) The electronic wave functions deviate from the ground state, and (ii) the ionic subsystem spontaneously decreases its temperature due to the energy transfer to the electrons. To counteract these two effects, we perform systematic electronic minimizations and control the ionic temperature by coupling the ionic subsystem to the Nosé thermostat. The frequency of the electronic optimizations depends closely on the rate of transfer of energy from the ionic to the electronic subsystem. In principle, electronic minimizations could be performed at every time step. This, however, would be rather costly, and in practice it is not necessary since, even in metals, by a convenient choice of μ the ionic trajectories obtained from Eqs. (5) deviate appreciably from the BO surface only after many time steps. By performing systematic electronic optimizations, the interparticle potential is not allowed to deviate appreciably from the BO surface all along a MD simulation run. Thus the conditions for the approximate sampling of the canonical distribution under Nosé dynamics remain valid also in this case.

In the present investigation of l-Si, we have performed a Nosé-type constant-temperature, constant-volume MD simulation at the experimental density $\rho = 2.59$ g cm^{-3}.[11] The MD cell contained 64 atoms with periodic boundary conditions of the simple cubic (sc) type. The average temperature was kept at $T = 1800$ K, close to the experimental melting point $T_m = 1680$ K.[10] At $T = 1800$ K our system was characterized by good liquidlike diffusive behavior. The present simulation does not allow a direct evaluation of the melting point of our model system. It is well known that large overheating and/or undercooling is present in molecular-dynamics simulations of small samples with periodic boundary conditions. In order to calculate accurately the melting point of our system, we should perform highly nontrivial and time-consuming free-energy evaluations, within our *ab initio* approach, for both the liquid and solid phases. Such calculations would allow to predict phase diagrams from first principles and are therefore an important challenge for the future.

We used nonlocal norm-conserving pseudopotentials of the Bachelet-Hamann-Schlüter type[21] with s nonlocality only. Kleinman and Bylander's factorized form[22] was adopted to speed up the calculation. Exchange and correlation effects were treated within LDA in the parametrized form of Ref. 23. The electronic orbitals were expanded in plane waves with an energy cutoff of 12 Ry. The Γ point, $\mathbf{k} = (0,0,0)$, only was used to sample the Brillouin zone (BZ) of the MD supercell. The integration time step was 5.5 a.u. $(1.3 \times 10^{-16}$ s), while the fictitious "mass" μ was taken to be 300 a.u. The dynami-

cal mass Q was set to 2.5×10^5 a.u. With this mass the oscillation periods of s are comparable to the inverse of the frequency of optical phonons in c-Si. In semiconducting phases this choice of parameters would have guaranteed a very accurate adiabatic evolution of the system over a relatively long MD run. In the present metallic-liquid phase, the system remains close to the BO surface only for times of the order of ~ 500 time steps. For this reason we performed periodic quenches of the electrons to the instantaneous ground state every 500 time steps. Toleration of small deviations from the BO surface corresponds to ascribing it a finite thickness. The average thickness of the BO surface in our simulation was less than 50 K, while the maximal thickness was ~ 100 K, small compared to the ionic temperature and also to the average temperature fluctuations, which in our small sample are of the order of 10% of the average temperature. By varying the rate of periodic electronic minimizations, we have checked that the accepted tolerated thickness of the BO surface in our simulation does not affect our measured properties in any noticeable way.

We note that, within our approach, one neglects thermal effects on the electronic Fermi surface, which is assumed to be perfectly sharp as at $T = 0$ K. This is a reasonable assumption, since at the temperatures of the simulation, the thermal smearing of the Fermi surface is small compared with the occupied-valence-band width.

The initial configuration was generated by starting from atoms in diamond lattice positions with small random displacements and electronic orbitals in the ground state. Then the system was heated up to ~ 6000 K by rescaling the velocities of the particles in order to achieve a fast onset of the diffusive behavior, signaling transition to a liquid phase. The temperature of the liquid structure was then reduced to $T = 1800$ K and the Nosé thermostat switched on. After equilibration, we have followed the system for a total time of 1.2 ps, sufficiently larger than the typical relaxation times.

We have checked the convergence of our calculation with respect to periodic boundary conditions, cell size, inclusion of p nonlocality in the pseudopotential, and energy cutoff in the plane-wave expansion of the electronic wave functions. The results were quite sensitive to variations in the energy cutoff, while changes in other conditions produced only minor effects. A cutoff of 12 Ry was necessary to achieve convergence and produce a coordination in close agreement with experiments. By lowering the cutoff we observed a reduced tendency toward metallization and a simultaneous trend toward more structured systems having lower average coordination. In particular, with an energy cutoff of 6 Ry we reproduced, with the 64-atom cell, the results already found in a preliminary calculation done with a 54-atom fcc cell and a similar cutoff.[7] The observed relative independence of the structural properties on the unit-cell size and shape provides an indication that the calculation of the interatomic forces, which requires a BZ average, is essentially converged with respect to $\mathbf{k}$-point sampling. A more detailed account of these convergence studies is given in the Appendix.

III. SHORT-RANGE ORDER AND ENERGETICS

We now turn to a detailed analysis of the structural properties of l-Si. In Fig. 1 we show the results obtained for the static structure factor $S(k)$ and the pair correlation function $g(r)$ and compare them with x-ray-[1] and neutron-[2] scattering experiments. The $g(r)$ is interrupted at the distance of ~ 10 a.u., which is the largest length we can study with our small-sized model. The agreement with experimental data is very favorable, especially if one considers the differences between the two sets of experimental data and the absence of any fitting parameter in the theory.

The structure of l-Si is dissimilar to that of most simple liquid metals.[5] The first peak of $S(k)$ is asymmetric, with a shoulder on the high-k side. There is a secondary maximum of $g(r)$ (at ~ 7 a.u.) that appears at the position where simple liquids have the first minimum. The average coordination number from the experimental $g(r)$ is 6.4. Not surprisingly, simple models such as hard spheres fail completely in the description of l-Si.[24] This is a situation where *ab initio* MD is particularly suitable because no arbitrary assumption is made on the interaction potential. Since the atomic correlations fall off rapidly in liquids, the effect of a relatively small size of the unit cell does not pose serious limitations on our structural model. In particular, the theory correctly predicts the shoulder on the first peak of $S(k)$, the anomalous secondary peak of $g(r)$, and the first peak position at ~ 4.65 a.u., appreciably larger than the value 4.44 a.u. in c-Si. The coordination number, as obtained by integrating $g(r)$ up to the first minimum $r_m = 5.85$ a.u., is ~ 6.5, in close agreement with the experimental value of ~ 6.4.[1,2] As shown in Fig. 2, our results indicate presence of a broad distribution of local coordinations dominated by the sixfold one.

Additional information on the short-range order (SRO) can be obtained from higher-order correlation functions. In our case the triplet correlations are particularly important since the system retains some covalent bonding effects and has directional forces. This is conveniently measured by the bond-angle distribution function $g_3(\theta, r_m)$. Here θ is the angle between the two vectors that join a central particle with two neighbors at a distance less than r_m. Our $g_3(\theta, r_m)$, shown in Fig. 3, is

FIG. 2. Distribution $d(N)$ of local coordinations in l-Si. The coordination shell is defined by r_m, the first minimum of $g(r)$.

rather broad with maxima centered at $\theta \sim 60°$ and $\sim 90°$.

In the past, various empirical models for SRO in l-Si have been proposed. They either assume presence of two kinds of atoms, differing in size[2,25] or coordination[1] (either fourfold covalent or 12-fold metallic), or suggest that SRO in l-Si is close to that of the β-tin or the sc structures,[14] which both are sixfold coordinated and metallic. Our results do not support these models. They indicate presence of a broad distribution of local coordinations and bond angles distinctly different from that of sc or β-tin.

Some microscopic models of l-Si are based on few-body potentials.[5,6,9,13] Two approaches have been widely used. Effective pair potentials, obtained from pseudopotential perturbation theory (PPT), have been extensively used by Hafner and collaborators to model a large class of liquid elements.[26] In an earlier application to Si, Hafner and Kahl[5] based their description of the liquid structure on the optimized random-phase approximation.[27] More recently, l-Si was simulated by Jank and Hafner using MD.[9] The resulting $S(k)$ and $g(r)$ were in good agreement with experiment. One should expect, however, that the perturbation-theory treatment, relying on weak pseu-
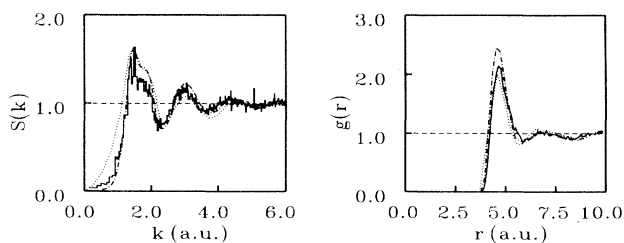

FIG. 1. $S(k)$ (left panel) and $g(r)$ (right panel) of l-Si. Solid line, MD simulation; dotted line, neutron-diffraction experiment (Ref. 2); and dot-dashed line, x-ray-diffraction experiment (Ref. 1).
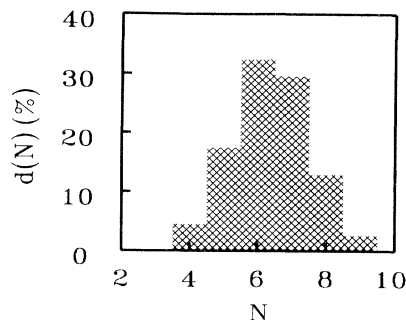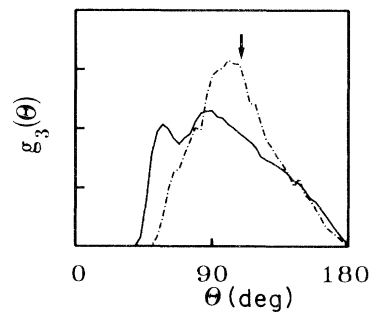

FIG. 3. Bond-angle distribution functions $g_3(\theta, r)$. The cutoff distance r is equal (a) to r_m, the first minimum of $g(r)$ (solid line), and (b) to r_c, the covalent cutoff defined in the text (dot-dashed line). The arrow indicates the position of the tetrahedral angle.

dopotentials and electron-gas screening, should be more appropriate for simple metals such as Na than for Si. In spite of its metallic character, the electronic charge density of l-Si is far from being uniform (see Sec. IV). The PPT potential is not able to stabilize the tetrahedral network and hence cannot be used to study solid phases. Stillinger and Weber[6] (SW) constructed an empirical potential for Si that includes two- and three-body terms and used it in a MD study of the liquid phase. Again, $S(k)$ and $g(r)$ were in agreement with experiments. Because of the inclusion of the three-body terms, the SW potential can stabilize the tetrahedral network. As a consequence, it has been widely used to construct structural models of liquid[6,28] and solid phases[28−31] of Si. We consider here the SW potential as a prototype of classical models tailored to describe systems with covalent bonds. By comparing our simulated structure with the SW liquid, we find that there are important qualitative differences between the two structures, in spite of the fact that the two liquids have basically the same static structure factor. Indeed, important differences between the two liquids appear in higher-order correlation functions, such as $g_3(\theta, r_m)$. This is shown in Fig. 4, where the SW g_3 is from Ref. 30. The angular correlations in the two liquids are quite different. In particular, in the SW liquid there is a strong tendency to overemphasize the local tetrahedral order. Such feature is not present in the PPT liquid whose $g_3(\theta, r_m)$ (Ref. 9) is very similar to ours.

Our simulation not only provides direct information on the microscopic structure of the liquid, but allows one also to compute specific thermodynamic properties such as internal energies, specific heats, etc. This opens the possibility of deriving thermodynamic phase diagrams of real materials from first-principles microscopic calculations. It is therefore interesting to assess the accuracy of the thermodynamic information that can be extracted from the simulation. An internal energy U is readily obtained as

$$U = \left\langle \frac{1}{2} \sum_I M_I \dot{\mathbf{R}}_I^2 + E[\{\psi_i\}, \{\mathbf{R}_I\}] \right\rangle , \tag{6}$$

where the brackets indicate temporal average over BO ionic trajectories. By performing a separate calculation for the crystal at $T=0$, with the same BZ sampling, pseudopotential, and plane-wave cutoff used for the liquid, we compute $\Delta U_{l\text{-}c} = U_l(T=1800\ \text{K}) - U_c(T=0\ \text{K})$. Using the experimental equilibrium volumes at standard pressure for both the liquid and crystal, we obtain $\Delta U_{l\text{-}c} \simeq 108.6$ kJ/mol. This value should be approximately equal to the corresponding enthalpy difference $\Delta H_{l\text{-}c} = \Delta U_{l\text{-}c} + p\,\Delta V$, since the contribution to enthalpy due to $p\,\Delta V$ is negligible. Using experimental data from Ref. 32 we obtain $\Delta H_{l\text{-}c}^{\text{expt}} \simeq 93.4 \text{kJ/mol}$, in very good agreement with our theoretical prediction.

IV. BONDING PROPERTIES

In our simulation we generate simultaneously the ionic trajectories and the corresponding ground-state electronic charge densities. Therefore, we can study directly the evolution of the chemical bonds resulting from atomic motion. In this way we have been able to put on a quantitative theoretical basis the concept of covalent bonding effects in l-Si. Persistence of transitory covalent bonding in the metallic-liquid phase of Ge was also suggested by Ashcroft,[33] on the basis of qualitative theoretical arguments.

A plot of the pseudo-charge-density $\rho_e(\mathbf{r})$ in a plane defined by three neighboring atoms in several liquid configurations is shown in Fig. 5, where for comparison we also report [in Fig. 5(a)] $\rho_e(\mathbf{r})$ in the (110) plane of crystalline silicon (c-Si). In Figs. 5(b) and 5(c) the distances between the two external atoms and the one at the
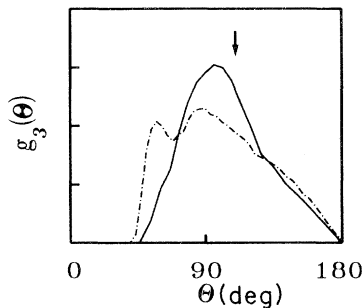

FIG. 4. Bond-angle distribution function $g_3(\theta, r_m)$ of the Stillinger-Weber (solid line, Ref. 30) and of our (dot-dashed line) l-Si. The arrow indicates the position of the tetrahedral angle.
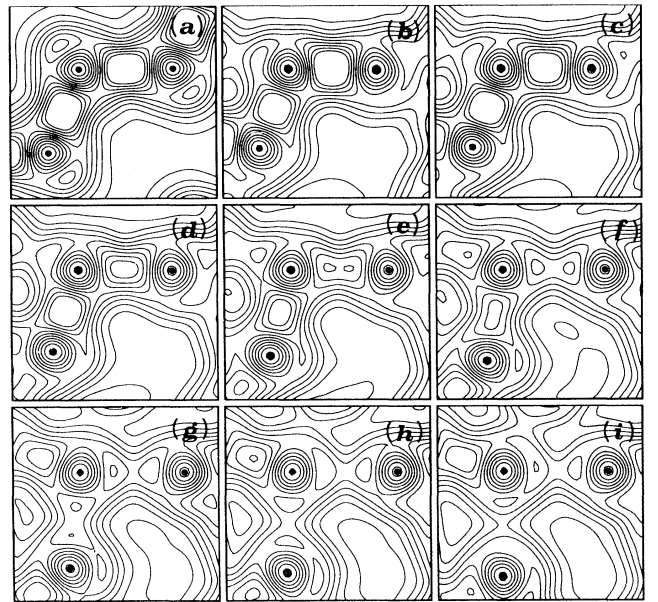

FIG. 5. Contour plots of the valence-electronic-charge density $\rho_e(\mathbf{r})$. (a) c-Si in the (110) plane. (b)–(i) Evolution of $\rho_e(\mathbf{r})$ in l-Si at time intervals of $\sim 5.5 \times 10^{-3}$ ps. The dots indicate the positions of the ions.

center are quite close to the bond length in c-Si. Correspondingly, the electronic densities have several common characteristics. Both in the crystal and liquid, $\rho_e(\mathbf{r})$ is strongly nonuniform and there is an accumulation of charge between pairs of adjacent atoms. This provides striking evidence for the persistence of covalent bonds in the liquid. Figure 5(b) shows a snapshot of an instantaneous local configuration which changes in time with the typical time scale of the diffusive motion of the atoms. Its subsequent evolution at intervals of time of $\sim 5.5 \times 10^{-3}$ ps is shown in Figs. 5(c)–5(i). We note that in Fig. 5(e) one of the two bonds of Fig. 5(b) starts to break, while the other is substantially weakened. Finally, in Fig. 5(i) both bonds have disappeared, while in the upper left corner one can guess the formation of a new bond with an incoming atom not shown in the picture. Interestingly, Fig. 5 also shows a correlation between covalent bonding and local tetrahedral order. When the atoms are covalently bonded as in Figs. 5(b) and 5(c) the angle between the two atomic pairs is close to tetrahedral ($\sim 109°$), while it is different when the bonds are broken.

To emphasize the chemical character of the bonding charge, we can take, for any liquid configuration, the difference between the true charge density and a superposition of atomic densities, i.e.,

$$\Delta\rho_e(\mathbf{r}) = \rho_e(\mathbf{r}) - \sum_I \rho_e^{\text{at}}(|\mathbf{r} - \mathbf{R}_I|) . \tag{7}$$

Here ρ_e^{at} denotes the pseudo-charge-density of the free atom. A plot of $\Delta\rho_e$ for the same liquid and crystalline configurations of Fig. 5 is shown in Fig. 6, confirming

that the pileup of charge is not just a consequence of the occasional close approach between two atoms, but reflects the formation of a chemical bond.

An extensive analysis shows that covalent bonds almost always form between pairs separated by a distance less than ~ 4.7 a.u. For larger separation distances the great majority of the bonds are broken. Therefore, we can define $r_c = 4.7$ a.u. as the cutoff distance for covalent bonds. This is slightly larger than the equilibrium bond length of 4.44 a.u. of c-Si. Only a fraction of $\sim 30\%$ of the atoms in the first peak of $g(r)$ are at distances less than r_c. The bond-angle distribution function $g_3(\theta, r_c)$ corresponding to these atoms is shown in Fig. 3. $g_3(\theta, r_c)$ is peaked around an angle close to tetrahedral. A similar, albeit considerably narrower, bond-angle distribution is found in amorphous silicon. The covalently bonded atoms tend to form chains of variable length. The presence in the liquid phase of local tetrahedral fluctuations may play an important role in explaining why silicon is able to reconstruct easily a tetrahedral network upon cooling.

The average properties of the covalent bonds in the liquid can be analyzed in the following way. According to the Phillips bond-charge model,[34] the pileup of charge, in a covalent bond in an elemental semiconducting crystal, can be mimicked by a point charge located at the bond center. We extend this concept to the liquid by associating a point charge to each local maximum of the valence electron density. We then consider these point charges, which we call bond charges (BC), as extra particles in our system and apply standard correlation-function techniques to characterize their average properties. For a given ionic configuration, the electronic density $\rho_e(\mathbf{r})$ has several local maxima. In order to locate them, we adopt a simulated annealing technique.[35] In our simulation $\rho_e(\mathbf{r})$ is defined on a uniform cubic mesh of spatial points which defines a three-dimensional lattice. We start a search from a randomly chosen lattice point. Then we generate a sequence of Monte Carlo moves between neighboring points according to the Metropolis algorithm,[36] taking the negative of the electronic density $\rho_e(\mathbf{r})$ as the cost function.[35] By starting at a high effective "temperature" and by subsequently reducing it, one ends up in a local maximum of ρ_e. A representative set of local maxima is generated by repeating the search several times with different starting conditions. The advantage of using a simulated annealing technique is that, by appropriate tuning of the annealing schedule, one can reduce the probability of finding weak maxima resulting from fluctuations due to disorder. As a consequence, the probability of finding strong maxima, representative of real chemical effects, is increased.

We locate the BC's for a representative subset of ionic configurations generated by MD and compute the partial pair correlation functions $g_{\text{BC-BC}}(r)$ (bond-charge–bond-charge) and $g_{I\text{-BC}}(r)$ (ion–bond-charge). The results are plotted in Fig. 7, where we report for comparison also the ion-ion correlation function $g_{I\text{-}I}(r) = g(r)$. $g_{I\text{-BC}}(r)$ is peaked at ~ 1.7 a.u., which does not correspond to half the distance between a pair of ions and has a characteris-
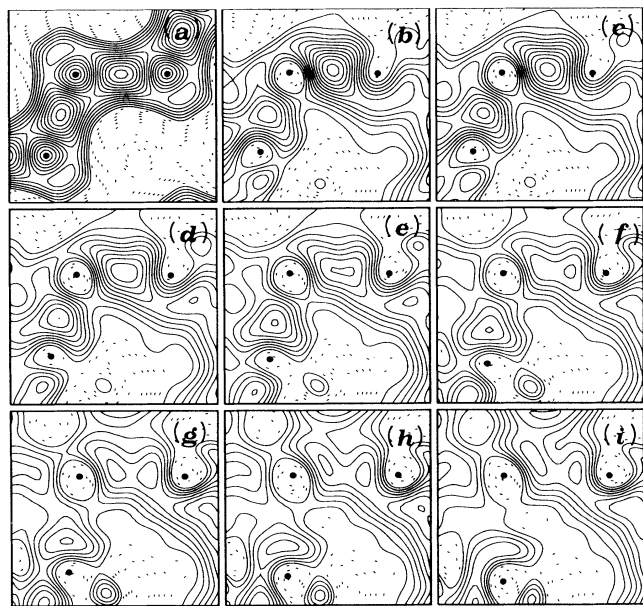

FIG. 6. Charge-density difference $\Delta\rho_e(\mathbf{r})$, as defined in the text, for the configurations of Fig. 5. Solid (dashed) lines indicate positive (negative) density. The atomic positions are indicated by the dots.
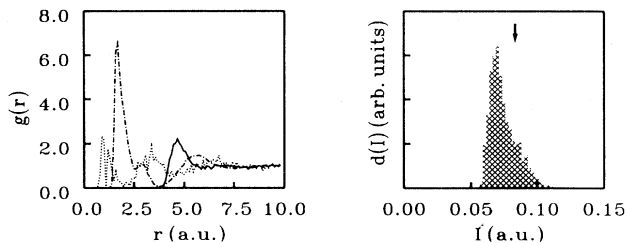
FIG. 7. Statistical characterization of bonding properties of *l*-Si. Left panel: partial correlation functions (see text) $g_{BC-BC}(r)$ (dotted line), $g_{I-BC}(r)$ (dot-dashed line), and $g_{I-I}(r)$ (solid line). Right panel: distribution $d(I)$ of valence charge maxima (associated with BC's). The symbol I stands for the intensity of the valence charge at a local maximum. The arrow indicates the intensity of the valence charge at the midbond maximum in *c*-Si.
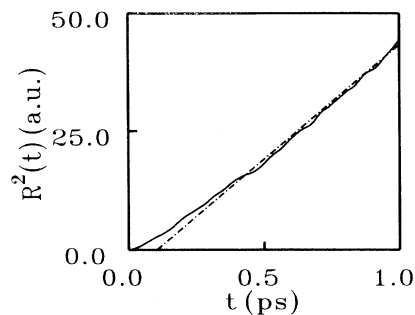

FIG. 8. Time dependence of the mean-square displacement $R^2(t)$ in *l*-Si (solid line). The least-squares fit to the asymptotic large-*t* behavior is shown by the dot-dashed line.

tic shoulder at ~ 3.0 a.u. However, the average value of the sum of the peak and shoulder positions corresponds closely to half the average ion-ion distance (first peak of g_{I-I}). This can be understood in terms of the existence of a substantial amount of broken (weak) bonds, since these are often characterized by the presence of two maxima in the charge density (cf. Fig. 5). Similarly, the peak at ~ 1 a.u. in $g_{BC-BC}(r)$ agrees with the distance between the two maxima of a broken bond. In Fig. 7 we also plot the distribution of the values of the local charge-density maxima. We see that a significant fraction of maxima is appreciably weaker than in *c*-Si. The tail on the high-density side of the distribution is due to compressed bonds.

We close this section by mentioning that a simple model based on the spirit of Phillips bond-charge model has been used recently to describe qualitatively the structure of *l*-Ge.[37]

V. ATOMIC DYNAMICS

MD generates atomic trajectories that allow one to study time-dependent phenomena and coefficients of atomic transport. This provides valuable information, since the dynamical properties of *l*-Si are essentially unknown. We limit here the analysis of our data to the diffusion constant D, the velocity autocorrelation function $Z(t)$, and its Fourier transform $Z(\omega)$, which gives the power spectrum of the system dynamics.

We have calculated the diffusion coefficient from the atomic mean-square displacement[38]

$$R^2(t) = \frac{1}{N} \sum_{I=1}^{N} [\mathbf{R}_I(t) - \mathbf{R}_I(0)]^2$$

$$\sim 6Dt + c, \quad \text{as } t \to \infty \ , \tag{8}$$

where D is the self-diffusion coefficient and c is a constant.[39] This is shown in Fig. 8. For long times, $R^2(t)$ exhibits a quasilinear behavior characteristic of a diffusive motion. Using formula (8), we extract $D \sim 2.26 \times 10^{-4}$ cm^2 s^{-1}. This value implies that, on average, in our simu-

lation each atom has traveled a distance of ~ 7 a.u. This means that a substantial part of the phase space has been sampled.

An alternative way of calculating D is by means of the velocity autocorrelation function (VACF), defined as

$$Z(t) = \frac{\langle \mathbf{v}(0) \cdot \mathbf{v}(t) \rangle}{\langle \mathbf{v}(0) \cdot \mathbf{v}(0) \rangle} \ . \tag{9}$$

In terms of the VACF, D is given by[38]

$$D = \frac{k_B T}{M} \int_0^\infty Z(t) dt \ . \tag{10}$$

Using Eq. (8) or (10) to compute D is mathematically equivalent. It is interesting, however, to see whether, in a numerical simulation, the two different procedures give the same results. In our case, using Eq. (10), we find $D \sim 2.02 \times 10^{-4}$ cm^2 s^{-1}, in good agreement with the result of Eq. (8). This value indicates a rather fast ionic diffusion. Although we are not aware of any direct experimental measurement of D for *l*-Si, our findings are consistent with indirect estimates based on the diffusivity of substitutional impurities such as P or Al.[40] The empirical SW potential yields $D \sim 6.94 \times 10^{-5}$ cm^2 s^{-1},[28] which is significantly smaller than our estimate.

The VACF is reported in Fig. 9. $Z(t)$ is always positive, leading to a high value of the diffusion coefficient, and has an oscillatory decay to zero after ~ 0.15 ps. This has to be contrasted with close-packed liquids such as Ar where a negative oscillation in $Z(t)$ is observed. This is believed to result from the caging effect of the shell of neighboring atoms.[38,39] *l*-Si is a much more open structure and exhibits no caging, but only effects due to the occasional formation of covalent bonds. A similar conclusion can be drawn also from the asymptotic behavior of the atomic mean-square displacement in Eq. (8). We find a negative value of ~ -5.09 a.u. for the constant c, which indicates that the diffusion is ahead of the corresponding Markovian process with no caging.

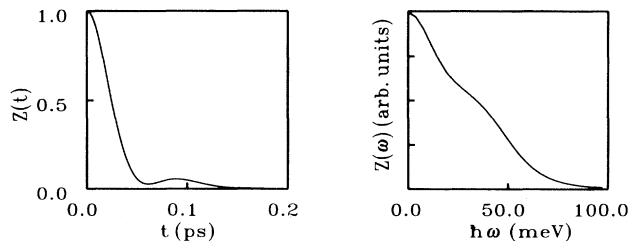The spectral density $Z(\omega)$ is obtained by taking the Fourier transform of the VACF:[38]

FIG. 9. Vibrational properties of l-Si. Left panel: velocity autocorrelation function $Z(t)$. Right panel: the corresponding power spectrum $Z(\omega)$.

$$Z(\omega) = \frac{2}{\pi} \int_0^\infty Z(t)\cos(\omega t)\,dt \ . \tag{11}$$

$Z(\omega)$ is shown in Fig. 9. Besides the low-frequency diffusive modes, one can identify vibrational modes reflecting covalent bonding effects. These can be associated with the shoulder of $Z(\omega)$ at the frequency of ~ 40 meV, which is quite close to the optical vibrational frequency of c-Si just below the melting point.[41]

In Fig. 10 we compare the power spectrum of the system dynamics resulting from our first-principles MD simulation with that of the SW liquid.[31] The two spectra are significantly different. In particular, the dynamics of the SW liquid bears a close resemblance with that of the corresponding crystal, as signaled by the presence of two broad peaks that are remnants of the crystalline acoustic and optical vibrational modes, respectively. This again indicates the tendency of the SW potential to overemphasize tetrahedral bonding.

VI. ELECTRONIC PROPERTIES

There are not many experimental data on the electronic structure of l-Si. As mentioned in the Introduction, metallic character results from measurements of both the dc (Ref. 10) and ac (Ref. 4) electrical conductivity. How-
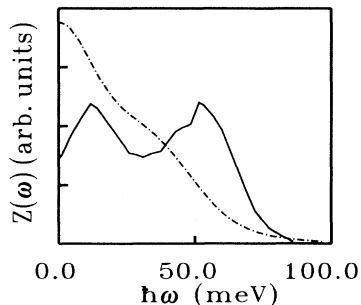

FIG. 10. Spectral density $Z(\omega)$ of the SW liquid (solid line, from Ref. 31) compared to the one of our simulation (dot-dashed line).

ever, detailed information on the occupied and unoccupied electronic density of states is missing. Only the partial density of p states in the valence band has been extracted from x-ray-emission experiments.[3] These data have been interpreted as indicating substantial free-electron-like behavior, with no sign of the sp mixing at the bottom of the band, which occurs in both the crystalline and amorphous phases.

On the theoretical side, a qualitative discussion on the density of states of l-Si was made by Gaspard et al.,[14] who assumed the geometric structure to be dominated by sixfold-coordinated atoms which were modeled by simple cubic (sc) and white tin (β-Sn) forms. More recently, studies based on more realistic structural models were performed by Allen and Broughton[8] and by Jank and Hafner.[9] All investigations agree in predicting metallic character. In particular, Allen and Broughton generated a SW liquid and used an empirical tight-binding model to calculate the density of states and the frequency-dependent electrical conductivity with a Kubo-Greenwood formula. In agreement with experiment, approximate Drude behavior was predicted, but the conductivity was severely underestimated by a factor of 3 over the entire frequency range, presumably due to nonsufficiently accurate momentum matrix elements. Jank and Hafner generated a liquid structure using a PPT potential. They limited their study to the electronic density of states, which was calculated with a self-consistent linear muffin-tin orbital (LMTO) procedure within the atomic-sphere approximation (ASA).[42] They used a liquid configuration generated by MD with a 64-atom cell with periodic boundary conditions, similarly to what is done in the present study. The result was an electronic density of states that looked remarkably free-electron like. Jank and Hafner analyzed also the effect of Brillouin-zone sampling on their density of states and found that, although some general features, such as e.g., the metallic character, are relatively insensitive to Brillouin-zone sampling, the use of the $\mathbf{k}=0$ point only may give rise to additional structures. On the other hand, a single special $\mathbf{k}$ point[43] is already enough to produce a density that is quite close to convergence.

In all these approaches, atomic and electronic structures are viewed as separate problems and are handled with different techniques. By contrast, in our scheme, atomic coordinates and corresponding electronic ground state are the result of a single and self-consistent procedure. Given the ground-state potential, occupied and unoccupied KS states can be calculated for each liquid configuration generated by MD. This makes possible to compute a large number of electronic properties, the BO adiabatic separation between electrons and ions being the only basic approximation. Here we limit our investigation to study the electronic density of states and the frequency-dependent electrical conductivity. In all the results that we present below, we have considered only the KS states at $\mathbf{k}=0$. This is fully consistent with the treatment of the electronic ground state that we adopted to dynamically generate the atomic configurations. On the other hand, this results in a poor energy resolution of the calculated spectral properties. It would be rather

straightforward (even if computationally more time consuming) to improve Brillouin-zone sampling in the calculation of spectral properties, as is customarily done in conventional electronic structure calculations for crystalline systems. This and similar other refinements are left for future work.

In Fig. 11 we report the single-particle electronic density of states $N(E)$ calculated by averaging over 12 atomic configurations well separated in time. These provide a representative sample of the liquid, as can be seen by considering the contribution of the occupied states only to $N(E)$, averaged over the entire MD trajectory, which is also reported in the same figure. $N(E)$ displays metallic behavior as evidenced by the absence of a gap at the Fermi level E_F. Considering the limited energy resolution of the histogram, $N(E)$ is remarkably free-electron like. We expect that these general features will not change with a more careful k-point sampling, whose main effect should be simply to produce a smoother curve. A metallic density of states for l-Si was also found in a previous simulation by two of us, using a 54-atom cell and an energy cutoff of 5.5 Ry.[7] This earlier result is also reported in Fig. 11. The differences between old and new data are somewhat enhanced by the different graphic presentation, but they reflect also some real differences between the two simulations. In particular, the old $N(E)$ appears more structured with the presence of three broad features in the occupied band, somewhat reminiscent of the three main peaks found in the valence band of c-Si. If these features were real, they would suggest substantial sp hybridization in the liquid state, contrary to the indication of x-ray-emission experiments.[3] In Ref. 9, Jank and

Hafner suggested that these features were spurious effects resulting from poor k-point sampling. We believe that this is only partially true, since the same Brillouin-zone sampling is also used to produce the new data in which the features are, to a large extent, washed out. The other effect that should be invoked to explain the more structured shape of the old $N(E)$ is the observed general tendency to produce less metallic liquids with a small energy cutoff. As we have already remarked, a low-energy cutoff gives also rise to a more structured pair correlation function $g(r)$ and, correspondingly, to a lower average coordination.

We now turn to the electrical conductivity. A good general discussion on the conductivity of metallic l-Si can be found in Allen and Broughton.[8] We follow their treatment. In the melt the current is carried both by electrons and charged ionic cores. The contribution of positive-ion cores to the current can be estimated from the Einstein formula

$$\sigma = \frac{(Ze)^2 \rho D}{k_B T} . \tag{12}$$

In our case the ionic charge Z is equal to 4, the density $\rho = 2.59$ g cm^{-3}, and D, the diffusion constant, as obtained from our MD simulation, is $\sim 2 \times 10^{-4}$ cm^2 s^{-1}. At the temperature $T = 1800$ K, formula (12) gives a conductivity of $\sim 1.8 \times 10^{-4}$ $(\mu\Omega$ cm$)^{-1}$, i.e., about two orders of magnitude smaller than the measured value, which for l-Si is $(1.0-1.3) \times 10^{-2}$ $(\mu\Omega$ cm$)^{-1}$. Hence the ionic contribution to the electric current is negligible. If nonadiabatic effects can be neglected, the electronic contribution to the conductivity $\sigma(\omega) = \frac{1}{3}[\sigma_{xx}(\omega) + \sigma_{yy}(\omega) + \sigma_{zz}(\omega)]$ may be evaluated by means of the following Kubo-Greenwood (KG) formula:[44]

$$\sigma_{xx}(\omega) = \frac{2\pi e^2 \hbar^2}{\Omega m^2} \left\langle \sum_i \sum_j f_i (1 - f_j) \frac{|M_{ij}^x|^2}{\omega} \right.$$

$$\left. \times \delta(\varepsilon_j - \varepsilon_i - \hbar\omega) \right\rangle . \tag{13}$$

Here the factor of 2 stands for double-spin occupancy, Ω is the unit-cell volume, the brackets indicate temporal average over the BO ionic trajectories, the indices i and j refer to instantaneous adiabatic KS states, f_i and f_j indicate the Fermi distribution function, and the matrix element M_{ij}^x is given by $\langle \psi_i | (-i\partial/\partial x) | \psi_j \rangle$.

In our calculation we have assumed $T = 0$ in the Fermi distribution function. This is consistent with our general treatment of the electronic ground state, as we have already discussed in Sec. II. We have checked, however, that inclusion of electronic temperature effects, by putting $T = 1800$ K in the Fermi distribution function in Eq. (13), only produces minor changes in the calculated $\sigma(\omega)$. We also note that the nonlocality of the ionic pseudopotential, appearing in the energy functional [Eq. (2)], entails a correction to the momentum matrix elements.[45] We have not calculated this correction, which is found to be small, albeit not negligible (of the order of 10%), in crystalline static calculations.[45] Additional corrections are expected from a proper treatment of the nonuniform
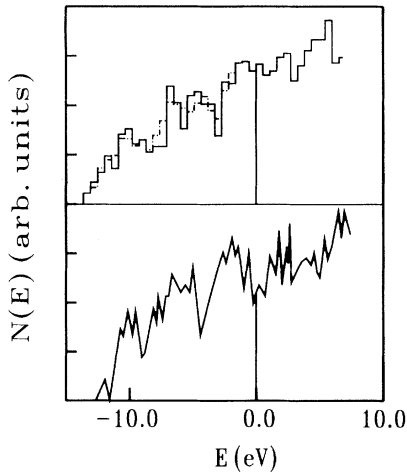

FIG. 11. Electronic properties of l-Si. Upper panel: density of Kohn-Sham eigenvalues $N(E)$ from the present calculation computed by (a) averaging over 12 configurations (solid line), and (b) averaging over the entire MD trajectory (dot-dashed line). The vertical line indicates the Fermi level E_F. Lower panel: density of Kohn-Sham eigenvalues $N(E)$ from a previous simulation (Ref. 7).

electronic charge density (giving rise to the so-called local-field effects[46]). Besides, a proper treatment of many-body effects would require the use of a Kubo[47] rather than a KG formula. In spite of all these approximations, use of Eq. (13) is substantially more accurate than the standard treatment adopted for the conductivity of liquid metals, i.e., Ziman theory.[48] Unlike Ziman theory, which requires weak-scattering conditions, the KG formula applies also to a strong-scattering environment when the electronic mean free path l is comparable to the interatomic spacing a. This is the situation of l-Si where, taking free-electron Fermi-gas parameters with $Z=4$, a mean free path $l \sim 4.5$ Å is estimated from the measured conductivity.[4] This is not large compared with the interatomic distance $a \sim 2.5$ Å.

We report, in Fig. 12, $\sigma(\omega)$ calculated by averaging over 12 ionic configurations. The finite width of the binds in the histogram reflects the finite-energy resolution of our spectral calculation. By extrapolating $\sigma(\omega)$ to $\omega \rightarrow 0$, we obtain $\sigma_{dc} = 0.38$ a.u. [0.0175 $(\mu\Omega\,cm)^{-1}$] in fairly good agreement with the experimental value of 0.27 a.u. [0.0124 $(\mu\Omega\,cm)^{-1}$].[10] The dc limit in our calculation has the largest uncertainty because the number of energy levels with $\varepsilon_i < E_F$ and $\varepsilon_j > E_F$ diminishes rapidly as $\omega \rightarrow 0$, causing a larger error bar in the low-ω sector of the histogram. Despite the short electronic mean free path, the calculated $\sigma(\omega)$ shows a Drude-like falloff. This behavior has been found also experimentally.[4] By fitting a Drude curve

$$\sigma(\omega) = \frac{\sigma(0)}{1 + \omega^2 \tau^2}$$

to our data in the range of the experimentally investigated photon energies (1.2–3.1 eV), we extract a relaxation time $(\tau^{theor})^{-1} \sim 2.93$ eV in close agreement with the value $(\tau^{expt})^{-1} \sim 2.99$ eV obtained by a Drude fit of the experimental data.[4] In view of the difficulties, mentioned above, involved in a first-principles calculation of the

electrical conductivity of a liquid metal such as Si, the overall good agreement with experiment is more than satisfactory.

An alternative simple estimate of σ_{dc} can be obtained from the following approximate expression, obtained by assuming the scattering to be so strong that $l \sim a$ (a being an average nearest-neighbor distance):[49]

$$\sigma_{dc} = \frac{S_F e^2 l g^2}{12\pi^3 \hbar} , \qquad (14)$$

with S_F being the area of the Fermi surface, l the mean free path, and $g = N(E_F)/N(E_F)_{free}$. This gives $\sigma_{dc} = 0.18$ a.u. [0.0083 $(\mu\Omega\,cm)^{-1}$], in reasonable agreement with both the KG formula and experimental data.

VII. CONCLUSIONS

We have presented an extensive molecular-dynamics study of l-Si, based on a fully *ab initio* approach, in which the interatomic potential is derived from the electronic ground state within DF theory. The scheme is parameter free and allows one to obtain both atomic and electronic properties of a molten system from a single self-consistent calculation.

The results for l-Si are rather encouraging. Structural and electronic properties are all in excellent agreement with the available experimental data. In addition, the calculation has revealed several important details of the microscopic dynamics that are presently not available from experiment. These refer, for instance, to the triplet correlations, the power spectrum of the system dynamics, and the self-diffusion coefficient. Perhaps the most important result of the present study has been obtained by analyzing the evolution of the valence electron density that accompanies atomic motion. This has revealed persistence of covalent bonding effects in l-Si, which manifest themselves through peculiar local tetrahedral fluctuations even though, on average, the majority of bonds are broken. These covalent fluctuations are intimately connected with the unusually open structure of metallic l-Si and the accompanying strongly nonuniform instantaneous valence-electronic-charge density.

In the last few years important progress in the understanding of l-Si has been made through MD simulations based on empirical or semiempirical effective classical potentials.[5,6,8,9,28–31] It is therefore quite interesting to compare the results of these approaches with those of our first-principles simulation. In this paper we have considered, in particular, the fully empirical SW model[6] and the semiempirical PPT model,[5,9] which is based on an approximate theoretical treatment. Our analysis has revealed that important qualitative differences exist between our liquid and the one resulting from the SW potential, both at the level of triplet correlations[30] and of dynamical properties.[31] Specifically, the tetrahedral character appears overemphasized in the SW model, due to the strength of the three-body interactions that are necessary to stabilize the crystalline network. In nature (and in our approach) the weakening of the directional interactions that accompanies melting is automatically accounted for by bond-breaking processes. On the other
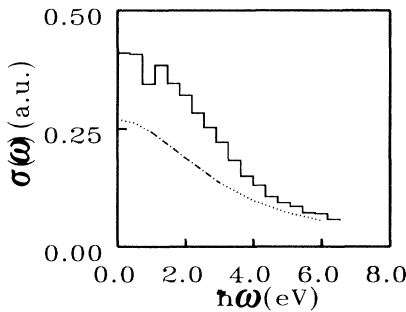
FIG. 12. Electrical conductivity $\sigma(\omega)$ as calculated from the Kubo-Greenwood formula given in the text (solid line). The result of a Drude fit of the experimental data from Ref. 4 is also reported (dot-dashed line). The Drude fit is from Ref. 4. The dotted line indicates an extrapolation of the Drude fit outside the range of the measured frequencies. Atomic unit of conductivity is used here $[e^2/\hbar a_B = 4.6 \times 10^6 \ (\Omega\,m)^{-1}]$.

hand, tetrahedral fluctuations are presumably missing in the PPT model,[5,9] which only contains central two-body interactions and, as a consequence, cannot be used to study phases different from liquid. Interestingly, the bond-angle distribution of the PPT model is very similar to that of our first-principles simulation. Dominance of central interactions in the liquid can be understood since the majority of bonds are broken. Nevertheless, particularly after seeing the nonuniform nature of the valence charge density, we found rather surprising that a good description of the structure of l-Si was possible within a model based on electron-gas screening. But perhaps this should not be considered surprising, since, after all, even c-Si is nearly free-electron like in many respects.[50] Clearly, a deeper assessment of the validity of perturbation theory is advisable. This should require a more detailed comparison with first-principles simulation data, including, e.g., dynamical properties.

The present study has been based on a constant-volume MD simulation in which the volume was assumed to coincide, somewhat arbitrarily, with the experimental equilibrium volume at the melting point. Constant-pressure MD simulations[51] are possible within the ab initio MD approach, as has been recently shown.[52] With constant-pressure simulations, the equilibrium volume of l-Si would be a result, rather than an input of the simulation, and it would be possible to check the prediction of the scheme for an important thermodynamic property such as the volume discontinuity at the melting point.

ACKNOWLEDGMENTS

FIG. 14. $S(k)$ (left panel) and $g(r)$ (right panel) of supercooled l-Si at $T \sim 1250$ K (Ref. 53). The data correspond to a fully converged cutoff of 12 Ry, and the averages are taken over a time of ~ 1 ps.

APPENDIX: DETAILS OF THE CONVERGENCE STUDY

We have carried out a convergence study of our l-Si calculation with respect to periodic boundary conditions, cell size, inclusion of p nonlocality in the pseudopotential, and energy cutoff in the plane-wave expansion of the electronic wave functions. The results were quite sensitive to variations in the energy cutoff. The variations in other parameters resulted only in minor changes.

The static structure factor and the pair correlation function obtained with an energy cutoff of 6 Ry is shown in Fig. 13. It appears that a low-energy cutoff produces a more structured system having lower average coordination. Interestingly, the 6-Ry structure is similar to a structure obtained in a preliminary calculation with a 54-atom fcc cell and a similar low-energy cutoff (5.5 Ry).[7] This structure is also reported in Fig. 13. On the other hand, a number of general qualitative features are common to the low-energy cutoff and the more accurate liquid structures. In particular, this is the case for triplet correlations, tetrahedral fluctuations, and metallic character of the electronic density of states. Further analysis
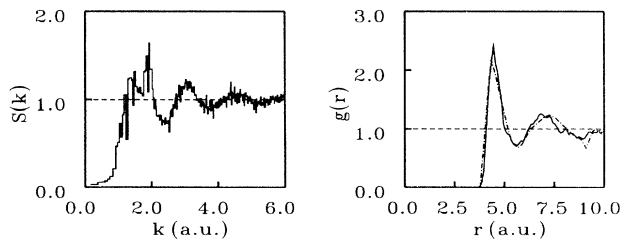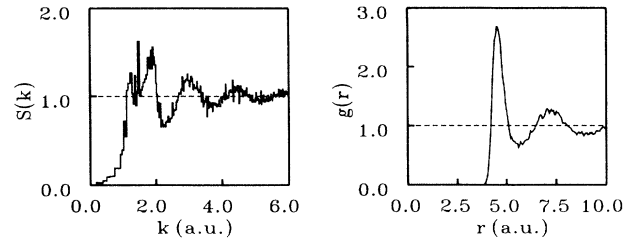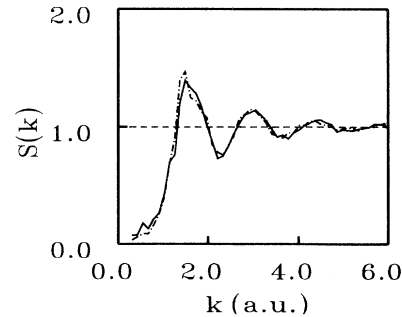

FIG. 13. $S(k)$ (left panel) and $g(r)$ (right panel) of l-Si ($T \sim 1800$ K) obtained with an energy cutoff of 6 Ry (solid line). The $g(r)$ of a l-Si sample obtained with a cutoff of 5.5 Ry, from a previous simulation (Ref. 7), is also shown for comparison (dot-dashed line). The present data are averaged over a time of ~ 0.6 ps.

FIG. 15. Effect of inclusion of p nonlocality in the pseudopotential on the $S(k)$ of l-Si. Solid line: both s and p nonlocality are included; dot-dashed line: only s nonlocality is included. In both calculations an energy cutoff of 12 Ry is used, and the averages are taken over a time of 1.2 ps. To facilitate the comparison, both curves have been smoothed.

reveals that the structure obtained with a low-energy cutoff is similar to the structure of a supercooled liquid, as it can be seen from Fig. 14, where we report the structural characteristics of a supercooled liquid, obtained with a converged energy cutoff of 12 Ry, at $T \sim 1250$ K.[53] The same conclusion about the similarity of a low-energy cutoff structure and a supercooled liquid is also supported by the reduced diffusion coefficient observed for the low-cutoff system.

The fact that, when using a very similar cutoff (6 and 5.5 Ry), the main short-range-order characteristics do not change on going from a 54 fcc to a 64 sc cell, provides an indication for a relative independence of the structural properties of our calculation with respect to unit-cell size and shape. This can be interpreted by say-

ing that the calculation of interatomic forces is reasonably converged with respect to BZ sampling. A more extensive test on the size dependence of the calculation would require simulations for larger system sizes, which have not been attempted so far.

In order to check the effect of the inclusion of p nonlocality in the pseudopotential, we have performed a liquid simulation run in which both s and p nonlocality were taken into account. The resulting static structure factor is compared in Fig. 15 with that obtained with a purely s-nonlocal pseudopotential. Since the structure is largely unaffected by the inclusion of p nonlocality, which, on the other hand, results in additional computational cost, we made the choice of using a purely s-nonlocal pseudopotential in all our subsequent calculations.

*Present address: Cavendish Laboratory (TCM) Madingley Road, Cambridge CB3 OHE, England.

[1]Y. Waseda and K. Suzuki, Z. Phys. B **20**, 339 (1975).

[2]J. P. Gabathuler and S. Steeb, Z. Naturforsch. A **34**, 1314 (1979).

[3]C. F. Hague, C. Sénémaud, and H. Ostrowiecki, J. Phys. F **10**, L267 (1980).

[4]K. M. Shvarev, B. A. Baum, and P. V. Geld, Fiz. Tverd. Tela (Leningrad) **16**, 3246 (1974) [Sov. Phys. Solid State **16**, 2111 (1975)].

[5]J. Hafner and G. Kahl, J. Phys. F **14**, 2259 (1984).

[6]F. H. Stillinger and T. A. Weber, Phys. Rev. B **31**, 5262 (1985).

[7]R. Car and M. Parrinello, in *Proceedings of the 18th Conference on Physics of Semiconductors*, edited by O. Engstrom (World Scientific, Singapore, 1987), p. 1169.

[8]P. B. Allen and J. Q. Broughton, J. Phys. Chem. **91**, 4964 (1987).

[9]W. Jank and J. Hafner, Phys. Rev. B **41**, 1497 (1990).

[10]V. M. Glazov, S. N. Chizhevskaya, and N. N. Glagoleva, *Liquid Semiconductors* (Plenum, New York, 1969).

[11]Y. Waseda, *The Structure of Non-Crystalline Materials; Liquids and Amorphous Solids* (McGraw-Hill, New York, 1980).

[12]T. E. Faber, *Introduction to the Theory of Liquid Metals* (Cambridge University Press, Cambridge, England, 1972).

[13]J. Tersoff, Phys. Rev. B **38**, 9902 (1988).

[14]J. P. Gaspard, Ph. Lambin, C. M. Moutet, and J. P. Vigneron, Philos. Mag. B **50**, 103 (1984).

[15]R. Car and M. Parrinello, Phys. Rev. Lett. **55**, 2471 (1985).

[16]See, for instance, *Theory of the Inhomogeneous Electron Gas*, edited by S. Lundqvist and N. H. March (Plenum, New York, 1983).

[17]I. Štich, R. Car, and M. Parrinello, Phys. Rev. Lett. **63**, 2240 (1989).

[18]R. Car and M. Parrinello, in *Simple Molecular Systems at Very High Density*, Vol. 186 of *NATO Advanced Study Institute, Series B: Physics*, edited by A. Polian, P. Loubeyre, and N. Boccara (Plenum, New York, 1989).

[19]W. Kohn and L. J. Sham, Phys. Rev. **140**, A1133 (1965).

[20]S. Nosé, Mol. Phys. **52**, 255 (1984); J. Chem. Phys. **81**, 511 (1984).

[21]G. B. Bachelet, D. R. Hamann, and M. Schlüter, Phys. Rev. B **26**, 4199 (1982).

[22]L. Kleinman and D. M. Bylander, Phys. Rev. Lett. **48**, 1425 (1982).

[23]J. P. Perdew and A. Zunger, Phys. Rev. B **23**, 5048 (1981).

[24]W. H. Shih and P. Stroud, Phys. Rev. B **31**, 3715 (1984).

[25]B. R. Orton, Z. Naturforsch. A **30**, 1500 (1975).

[26]J. Hafner, *From Hamiltonians to Phase Diagrams. The Electronic and Statistical-Mechanical Theory of sp-bonded Metals and Alloys*, edited by M. Cardona, P. Fulde, K. von Klitzing, and H.-J. Queisser, Springer Series in Solid State Sciences, Vol. 70 (Springer, Berlin, 1987).

[27]H. C. Andersen and D. Chandler, J. Chem. Phys. **53**, 547 (1970); H. C. Andersen and D. Chandler, *ibid.* **57**, 1918 (1972).

[28]J. Q. Broughton and X. P. Li, Phys. Rev. **35**, 9120 (1987).

[29]M. D. Kluge, J. D. Ray, and A. Rahman, Phys. Rev. B **36**, 4234 (1987).

[30]W. D. Leudtke and U. Landman, Phys. Rev. B **37**, 4656 (1988).

[31]W. D. Leudtke and U. Landman, Phys. Rev. B **40**, 1164 (1989).

[32]*Physics of Group IV Elements and III-V Compounds,* edited by K.-H. Hellwege and O. Madelung, Numerical Data and Functional Relationship in Science and Technology, Landolt-Börnstein, New Series, Group III, Vol. 17, Subvolume a (Springer-Verlag, Berlin, 1982).

[33]N. W. Ashcroft (unpublished).

[34]J. C. Phillips, *Bonds and Bands in Semiconductors* (Academic, New York, 1973).

[35]S. Kirkpatrick, C. D. Gelatt, Jr., and M. P. Vecchi, Science **220**, 671 (1983).

[36]N. Metropolis, A. Rosenbluth, M. Rosenbluth, A. Teller, and E. Teller, J. Chem. Phys. **21**, 1087 (1953).

[37]A. Ferrante and M. P. Tosi, J. Phys. Condens. Matter **1**, 1679 (1989).

[38]J. P. Hansen and I. R. McDonald, *Theory of Simple Liquids* (Academic, London, 1976).

[39]C. A. Croxton, *Liquid State Physics* (Cambridge University Press, Cambridge, England, 1974).

[40]*Technology of Si, Ge, and SiC,* edited by K.-H. Hellwege and O. Madelung, Numerical Data and Functional Relationship in Science and Technology, Landolt-Börnstein, New Series, Group III, Vol. 17, Subvolume c (Springer-Verlag, Berlin, 1984).

[41]C. Z. Wang, C. T. Chan, and K. M. Ho, Phys. Rev. B **39**, 8586 (1989).

[42]O. K. Andersen, O. Jepsen, and D. Glötzel, in *Highlights of Condensed Matter Theory*, edited by F. Bassani, F. Fumi, and

M. P. Tosi (North-Holland, Amsterdam, 1985); H. L. Skriver, *The LMTO Method,* edited by M. Cardona, P. Fulde, and H.-J. Queisser, Springer Series in Solid State Sciences, Vol. 41 (Springer, Berlin, 1984).

[43]A. Baldereschi, Phys. Rev. B **7**, 5212 (1973).

[44]E. N. Economou, *Green's Functions in Quantum Physics,* edited by M. Cardona, P. Fulde, and H.-J. Queisser, Springer Series in Solid State Sciences, Vol. 7 (Springer, Berlin, 1983), p. 152ff.

[45]S. Baroni and R. Resta, Phys. Rev. B **33**, 7017 (1986); M. S. Hybertsen and S. G. Louie, *ibid.* **35**, 5585 (1987).

[46]S. L. Adler, Phys. Rev. **126**, 413 (1962).

[47]See, for instance, G. Rickayzen, *Green's Functions and Condensed Matter* (Academic, London, 1980).

[48]See, for instance, J. M. Ziman, *Principles of the Theory of Solids* (North-Holland, Amsterdam, 1981), p. 415.

[49]N. F. Mott and E. A. Davis, *Electronic Processes in Noncrystalline Materials* (Clarendon, Oxford, 1979), p. 182.

[50]R. M. Martin, Phys. Rev. **186**, 871 (1969).

[51]H. C. Andersen, J. Chem. Phys. **72**, 2384 (1980).

[52]F. Buda, R. Car, and M. Parrinello, Phys. Rev. B **41**, 1680 (1990).

[53]I. Štich, R. Car, and M. Parrinello, Phys. Rev. B (to be published).